McCall *et al. Journal of NeuroEngineering and Rehabilitation* (2024) 21:146
https://doi.org/10.1186/s12984-024-01444-4

Journal of NeuroEngineering and Rehabilitation

RESEARCH Open Access

Soft pneumatic actuators for pushing fingers into extension

James V. McCall[1], Gregory D. Buckner[2] and Derek G. Kamper[1,3*]

Abstract

Background Compliant pneumatic actuators possess many characteristics that are desirable for wearable robotic systems. These actuators can be lightweight, integrated with clothing, and accommodate uncontrolled degrees of freedom. These attributes are especially desirable for hand exoskeletons, where the soft actuator can conform to the highly variable digit shape. In particular, locating the pneumatic actuator on the palmar side of the digit may have benefits for assisting finger extension and resisting unwanted finger flexion, but this configuration requires suppleness to allow digit flexion while retaining sufficient stiffness to assist extension.

Methods To meet these needs, we designed an actuator consisting of a hollow chamber long enough to span the joints of each digit while sufficiently narrow not to inhibit finger adduction. We explored the geometrical design parameter space for this chamber in terms of shape, dimensions, and wall thickness. After fabricating an elastomer-based prototype for each actuator design, we measured active extension force and passive resistance to bending for each chamber using a mechanical jig. We also created a finite element model for each chamber to enable estimation of the impact of chamber deformation, caused by joint rotation, on airflow through the chamber. Finally, we created a prototype hand exoskeleton with the chamber parameters yielding the best outcomes.

Results A rectangular cross-sectional area was preferable to a semi-obround shape for the chamber; wall thickness also impacted performance. Extension joint torque reached 0.33 N-m at a low chamber pressure of 48.3 kPa. The finite element model confirmed that airflow for the rectangular chamber remained high despite deformation resulting from joint rotation. The hand exoskeleton created with the rectangular chambers enabled rapid movement, with a cycle time of 1.1 s for voluntary flexion followed by actuated extension.

Conclusions The developed soft actuators are feasible for use in promoting finger extension from the palmar side of the hand. This placement utilizes pushing rather than pulling for digit extension, which is more comfortable and safer. The small chamber volumes allow rapid filling and evacuation to facilitate relatively high frequency finger movements.

Keywords Pneumatic actuators, Soft exoskeleton, Hand, Extension

*Correspondence:
Derek G. Kamper
dgkamper@ncsu.edu
[1]Joint Department of Biomedical Engineering, University of North Carolina at Chapel Hill, North Carolina State University, Chapel Hill, NC 27599, USA
[2]Department of Mechanical and Aerospace Engineering, North Carolina State University, Raleigh, NC 27695, USA
[3]Closed-loop Engineering for Advanced Rehabilitation Research Core, University of North Carolina at Chapel Hill, North Carolina State University, Raleigh, NC 27695, USA

Background

Hand impairment is a common occurrence following injury to the central nervous system. Substantial hand motor deficits are likely to occur after stroke [1], the most common cause of major long-term disability in the U.S. and a primary cause of disability throughout the world [2, 3]. Hand deficits are also associated with cerebral palsy (CP) [4, 5], the most common movement disorder in children [6, 7]. Reduced motor control of the hand has ramifications for self-care, employment, and social interactions.

In these clinical populations, common therapeutic practice for upper extremity rehabilitation involves repetitive practice of movement [8, 9] (e.g., constraint-induced movement therapy [10–12] and HABIT [13, 14]). Exoskeletons can facilitate this practice by providing assistance of desired movement [15, 16] and resistance of undesired movement. These devices typically employ rigid actuators, however, that may introduce considerable mass and inertia, potentially disturbing control and movement of the hand. Soft actuators have advantages in terms of weight, comfort, and conformation to different shapes [17–20]. These actuators may be especially well suited to the hand, where space is limited, additional mass is costly, and there are many degrees of freedom.

Many individuals with hand impairment especially have difficulty independently moving their digits. Therapeutic practice of finger individuation is needed and could be promoted by soft hand exoskeletons. Current soft actuator designs for the hand, however, are typically focused on pushing the digits into flexion from the dorsal side using a bellows-type approach [18, 21–23]. For stroke survivors or individuals with CP, finger extension is typically affected to a greater degree than digit flexion [24]. Involuntary coactivation of finger flexor muscles and muscle compartments leads to involuntary flexion of multiple fingers when trying to move only one digit [25]. Thus, active assistance of desired extension and resistance of unwanted flexion may be preferable to assistance of flexion for facilitating task practice. For rehabilitation therapy, the degree of assistance/resistance would ideally be variable and customized to each digit. Additionally, directly driving the finger without the need for external transmission, such as linkages or cables required with some solutions such as McKibben actuators [26], would be beneficial in order to reduce bulk and the number of required components, while increasing comfort. Furthermore, to facilitate therapeutic practice, the provided assistance should allow rapid, independent movement of the digits.

Given these target design criteria, we focused on palmar placement of the actuators, which would directly push (rather than pull) the digits into extension. Pushing reduces compressive joint forces relative to pulling while avoiding rubbing over the joints as the finger flexes. Rigid finger actuators have been positioned on the palm in the past to provide finger extension, but their presence limits finger flexion and precludes grasping of objects [27]. Similarly, stiffer pneumatic actuators such as PneuNets [28] could impose substantial resistance to desired flexion. Formerly, we developed polyurethane-based actuators that could assist digit extension from the palmar surface of the hand [29, 30]. When deflated, the actuators provided little added bulk or flexion resistance. The polyurethane actuators, however, are difficult to fabricate and are susceptible to kinking when bent, reducing airflow and the assistance provided.

The goal of this work was to design and test elastomer-based pneumatic chambers that could directly aid finger extension and resist unwanted flexion for each digit independently from the palmar side of the hand. To explore the design space, we evaluated a set of chambers with varying geometric characteristics: shape, size, and wall thickness. Each chamber was tested over a range of pressures and bending angles. Finite element models (FEMs) were created to estimate airflow through the chamber, as the airflow, and thus assistance provided to the finger, can become compromised as the chamber is distorted during finger flexion. These actuators were then incorporated into a soft glove designed to facilitate therapeutic practice of hand movements, including object grasp-and-release and rapid individuated movements of the digits. We hypothesized that a rectangular cross-sectional shape would yield higher extension force, higher flow rate, and lower passive bending resistance than a semi-obround shape, and that the extension force produced would increase with increased pressure and bending angle. A preliminary analysis of initial experimental results was presented in a conference paper [31].

Methods

Actuator design & fabrication

Pneumatic chambers were designed in SolidWorks (Dassault Systèmes, France) and manufactured using 3D printed custom molds [31]. DS20 (Dragon Skin 20, Smooth-On, Inc., US) was selected for the channel material based on its ability to resist pressure compared to other silicone rubbers [17] together with its excellent compliance to imposed bending. Fourteen different chambers were created, representing combinations of cross-sectional shape (semi-obround or rectangular), wall thickness, and actuator width and depth.

Rectangular and semi-obround cross-sections were selected based on successful application in other pneumatic actuators [32, 33] and on preliminary testing [31] that identified these shapes as capable of generating high extension force while offering limited resistance to bending. The semi-obround and rectangular chambers were

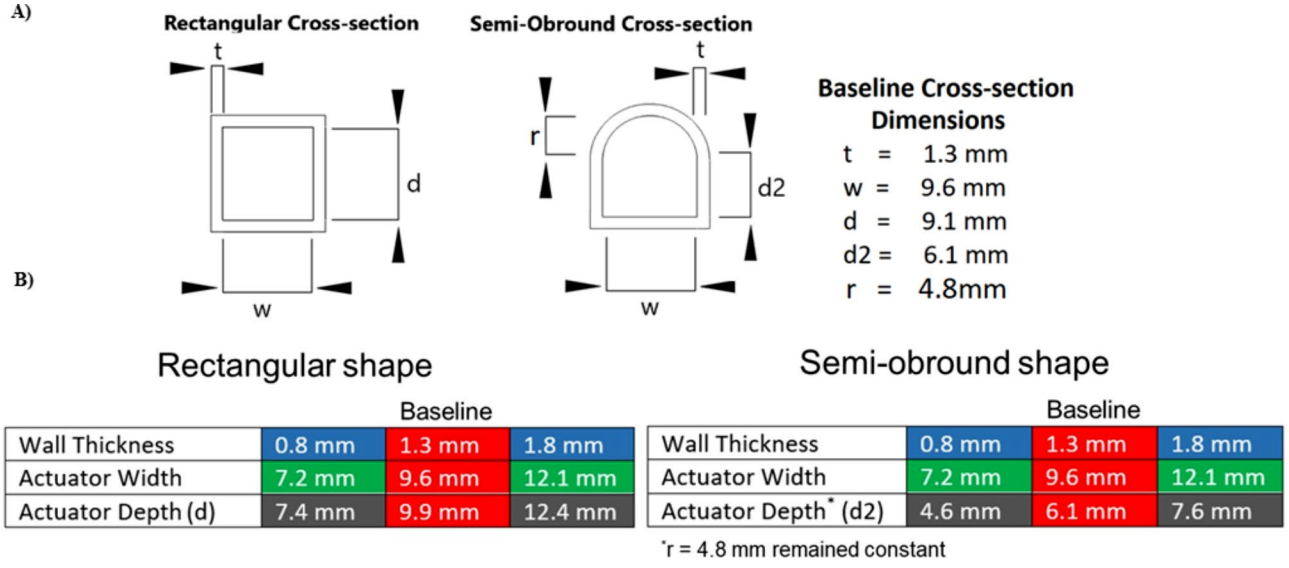

Fig. 1 Actuator Design and Dimensions. **A**) Cross-sectional dimensions of the baseline rectangular and semi-obround actuators. **B**) Dimensional variations used to create seven different actuators for each cross-sectional shape

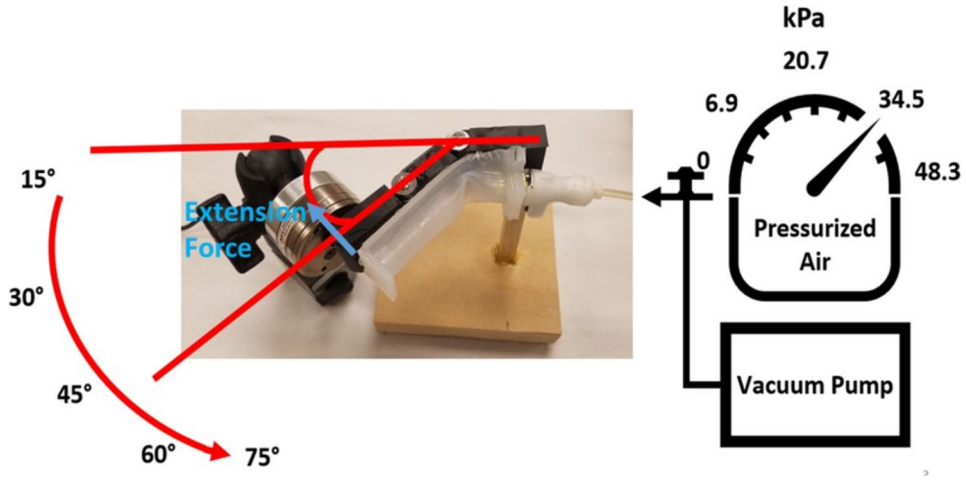

Fig. 2 Actuator and Test Fixture. Semi-obround actuator in actuator test setup with load cell and jointed fixture. Joint angle range and pressure range indicated

fabricated with the same cross-sectional widths and similar cross-sectional areas to facilitate direct comparison. The baseline dimensions for rectangular actuator wall thickness, width, and depth were: 1.3 mm, 9.6 mm, and 9.9 mm, respectively, while for the semi-obround shape, the baseline values were 1.3 mm for wall thickness, 9.6 mm for channel width, and a channel depth consisting of two components, d2=6.1 mm and r=4.8 mm (see Fig. 1). Parameter values were scaled by 75% and 125% of these baseline values (Fig. 1b). For the semi-obround shape, the d2-term was scaled for different depths while the r-term was kept constant. Thus, seven variations were created for each shape.

Actuator extension force (normal to the long-axis of the chamber/finger) and passive bending resistance were measured using a fixture which mimicked articulation of a 7.6 cm-long finger about the metacarpophalangeal joint (Fig. 2). The tip of this fixture was placed in contact with a force/torque sensor (Mini40, ATI Industrial Automation, Inc., US) positioned perpendicular to the long axis of the fixture. Actuator pressure was computer-controlled through a digital-to-analog converter (USB-3101, Measurement Computing, US) and an electropneumatic servo valve (Proportion Air, US). Actuators were tested at five bending angles (15°, 30°, 45°, 60°, and 75°). For extension force, actuators were tested at five pressures with respect to atmospheric pressure (0, 6.9, 20.7, 34.5, and 48.3 kPa). For the passive bending, the samples were tested at atmospheric pressure and with an applied vacuum.

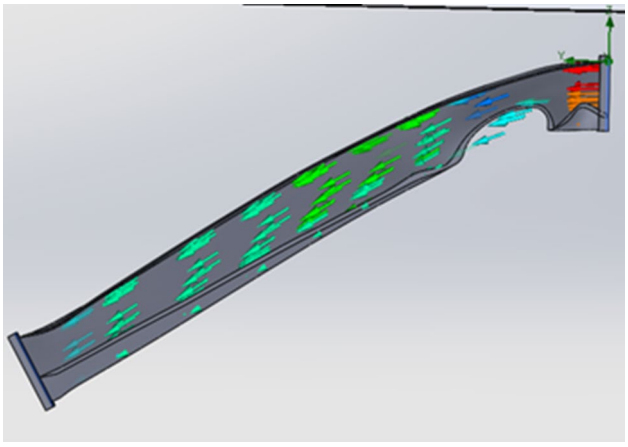

Fig. 3 Finite Element Model (FEM) Simulation. Cross-section of an FEM of an actuation chamber after deflection. Post-deformation flow trajectories are visible

Chamber simulation

To analyze airflow and chamber deformation of our actuators, we created an FEM of each actuator chamber within SolidWorks. Each chamber was represented by 10,000 tetrahedral elements; the elements were modeled as linear, elastic, and isotropic. Simulations were examined to estimate channel deformation during flexion, as would occur during hand closing due to the intended palmar placement of the actuator. Passive bending resistance was recorded for 15° and 30° of flexion (Fig. 3). These passive resistance values were compared to the experimental measurements taken with the actual specimens to examine validity of the model. Then, the minimum channel diameter and airflow rate for an imposed pressure of 34.5 kPa were obtained from simulation for each chamber across a range of flexion angles: 6°, 12°, 18°, 24°, 30°.

Hand Exoskeleton prototype

A soft, pneumatically actuated hand exoskeleton was then fabricated using five of the air chambers (one for each digit). Each chamber spanned the entire digit to provide extension assistance to all three joints (Fig. 4a). The chambers were placed inside Lycra sleeves which were attached to a golf glove (Fig. 4b). The glove allowed voluntary flexion (Fig. 4c) while actively assisting finger extension and resisting unwanted flexion. Operational bandwidth of the device was assessed by measuring force production delays and finger flexion/extension cycling time while a participant (one of the authors) wore the glove. Force generation delay was measured with the actuator at a 45° bending angle. With the wearer's fingers remaining passive, the actuator was pressurized with a step increase for each of the following levels: 6.9, 20.7, 34.5, and 48.3 kPa. We determined the rise time required for the force to reach 95% of the steady-state target value.

Lastly, we measured how rapidly digit flexion/extension cycles could be completed by an individual able to flex their fingers but with limited ability to extend them, such as might be the case for a stroke survivor. The user flexed a finger joint to an angle of 80°. This triggered pressurizing of the channel and thus extension of the finger. Once the finger was extended to an angle of less than 10°, the channel was allowed to depressurize and the user repeated the flexion/extension cycle.

Data analysis

Repeated measures ANOVAs were performed for both the empirically obtained data and simulation data using SPSS (IBM, Armonk, New York) to determine the effects of the between-sample actuator characteristics (shape, width, depth, and wall thickness) on extension force. For the extension force data, joint angle and actuator pressure comprised the within-sample factors. Evidence of a significant effect led to post-hoc Tukey tests to examine

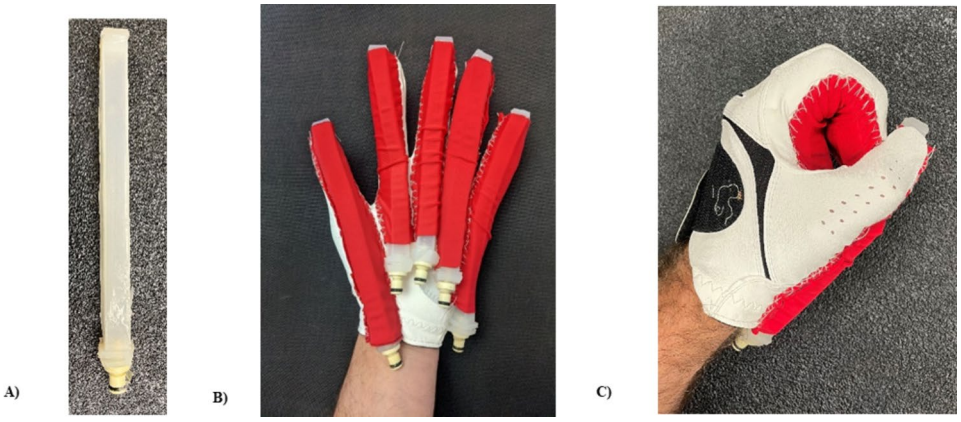

Fig. 4 Hand Exoskeleton Prototype for Left Hand. **A**) Single elastomeric actuator (DS20). **B**) Five chambers inserted into Lycra sleeves attached to the palmar side of an athletic glove. Extended posture. **C**) Flexed hand. Chambers not pressurized for these images

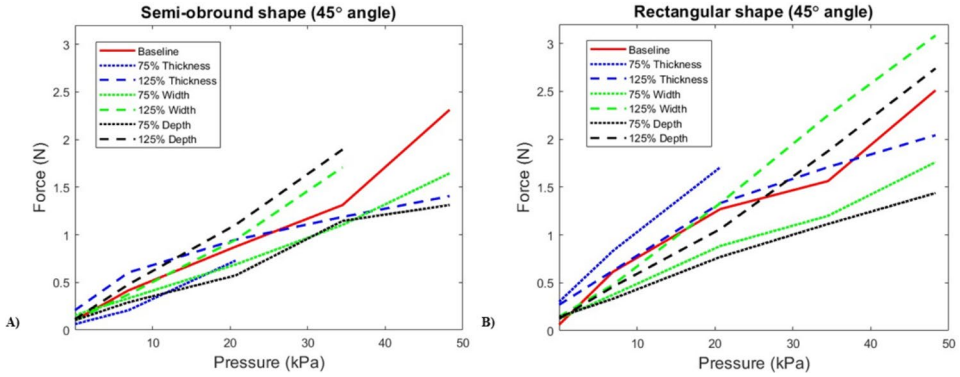

Fig. 5 Extension Force over Range of Pressures. The extension force created by different actuators at a joint rotation of 45° of flexion across a range of pressures. **A**) 7 permutations of actuators with semi-obround shape. **B**) 7 permutations of actuators with rectangular shape. Blue: different channel thicknesses; Green: different channel widths; Black: different channel depths. Dotted lines: smallest parameter value; Dashed lines: largest value; Solid red line: baseline (medium values). Missing data points arose from specimens exhibiting excessive deformation at those pressures

differences among levels of the significant independent factor. This procedure was repeated for the dependent variable of the fingertip force resulting from passive resistance to bending the actuator. To validate the simulation results, Pearson correlation coefficients were computed between the passive bending resistances and extension forces of the empirical and simulated data.

Results

Impact of wall thickness

The fourteen actuators, one for each set of parameters, were fabricated out of DragonSkin 20. After fabrication, uniformity of wall thickness was measured in three chambers with different nominal wall thicknesses with calipers. The actual wall thicknesses for the targeted values of 0.8 mm, 1.3 mm, and 1.8 mm for each chamber were (mean±standard deviation): 0.78±0.05 mm, 1.22±0.06 mm, and 1.82±0.04 mm, respectively. On average, the mean wall thickness was within 0.04 mm of the desired value and the standard deviation did not exceed 0.06 mm.

Active extension force

The actuators with a 0.8-mm wall thickness were unable to withstand pressures greater than 20.7 kPa, so these chambers were excluded from the extension force analyses. Across the remaining actuators, shape significantly affected extension force ($p=0.04$, $\eta p^2=0.60$), with greater extension forces produced with the rectangular chamber shape (1.0±0.98 N) than for the semi-obround shape (0.7±0.74 N) across all parameters, pressures, and angles (Fig. 5). The effect of chamber depth approached significance ($p=0.07$, $\eta p^2=0.65$); the greatest depth generated 0.50 N more force than the smallest depth. Neither thickness nor width significantly impacted force.

The within-sample factors of pressure and force also significantly affected extension force ($p=0.04$, $\eta p^2=0.58$; $p<0.01$, $\eta p^2=0.84$, respectively). Extension force for a given chamber increased up to the testing limit of 48.3 kPa (Fig. 6). Force also tended to increase with increasing joint angle, although excessive deformation occurred at the largest pressures and flexion angles for some specimens. For purely elastic deformation, a peak extension force of 3.6 N (generating 0.33 N-m of joint torque) was obtained for the rectangular shape with the 1.8-mm wall thickness at 60° of flexion and 48.3 kPa of pressure.

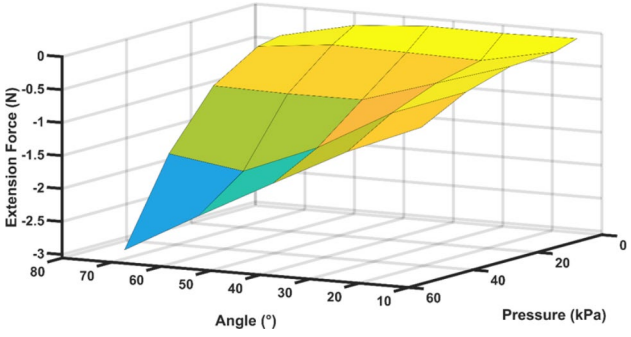

Fig. 6 Generated Extension Force. Surface plot of extension force as function of bending angle and chamber pressure. Values are averaged across actuators. Color mapping is associated with actuator force – yellow: no extension force created by actuator; blue: actuator extension forces of 3 N

Passive bending resistance

We examined the chamber resistance to imposed passive bending across all of the samples with the within-sample factor of flexion angle and the between-sample factors of shape, wall thickness, depth, and width. Resistance was measured for two pressures: atmospheric and vacuum. At atmospheric pressure, the between-sample effects of shape ($p=0.03$, $\eta p^2=0.60$) and wall thickness ($p=0.03$, $\eta p^2=0.71$) significantly impacted resistance. Passive bending resistance averaged 0.2 N for the rectangular chambers and 0.09 N for the semi-obround chambers

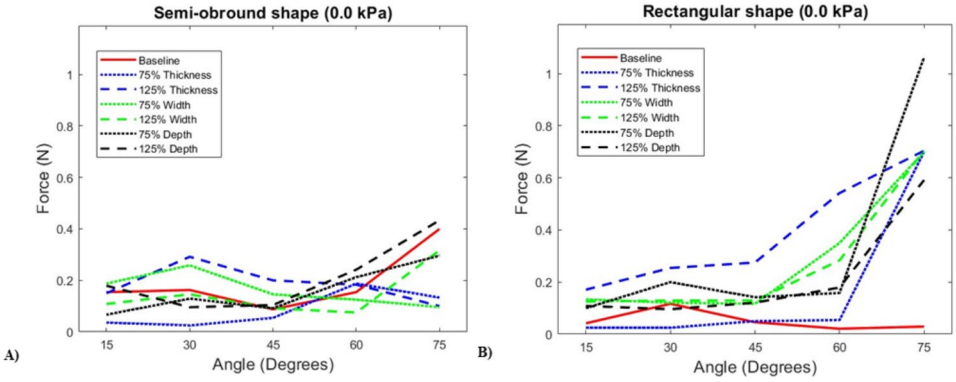

Fig. 7 Passive Bending Resistance over Range of Flexion Angles. **A**) 7 permutations of actuators with semi-obround shape. **B**) 7 permutations of actuators with rectangular shape. Blue: different channel thicknesses; Green: different channel widths; Black: different channel depths. Dotted lines: smallest parameter value; Dashed lines: largest value; Solid red line: baseline (medium values)

across all conditions and was, on average, 0.21 N higher for actuators with 1.8-mm thick walls than for those actuators with 0.8-mm wall thickness. There was no significant change in resistance due to actuator depth or width ($p>0.6$). Resistance tended to increase with flexion angle, especially for the rectangular shape (Fig. 7).

Applying the vacuum reduced the passive bending resistance by an average of 0.15 ± 0.08 N. Under vacuum, the thickness, depth, and width of the chambers had significant effects on the force needed to bend the chamber ($p=0.01$, $p=0.02$, $p=0.04$; $\eta p^2=0.86$, $\eta p^2=0.72$, $\eta p^2=0.64$, respectively). Passive bending resistance was smaller for the actuators with 1.3-mm thick walls than for those with other wall thicknesses ($p<0.01$), and for actuators with baseline depth as compared to those with the smallest depth ($p=0.02$).

Finite element simulation of airflow through chamber

The FEMs were first validated for passive response to bending through comparison with experimental data. Simulations of passive bending were performed at 15° and 30° of flexion for all 14 actuator iterations. Across cross-sectional shape, wall thickness, and chamber depth, and width, the Pearson correlation analyses revealed significant agreement between the empirical and simulation data (15°: $R=0.659$, $p=0.001$; 30°: $R=0.606$, $p=0.022$). We performed further simulations of active inflation at 15° of chamber flexion for 20.7 kPa of pressure for all 14 models. For this condition, the Pearson correlation between simulated and empirical extension forces was positive ($R=0.452$) and approached significance ($p=0.105$).

The ANOVA performed on simulation data from actuators across the range of simulated bending angles (0–30°) indicated that shape and depth had a significant effect ($p=0.043$, $\eta p^2=0.523$; $p=0.001$, $\eta p^2=0.896$, respectively) on minimum cross-sectional diameter. The minimum diameter was significantly greater, by an average of 3.8 mm, for the largest actuator depth (125% of baseline)

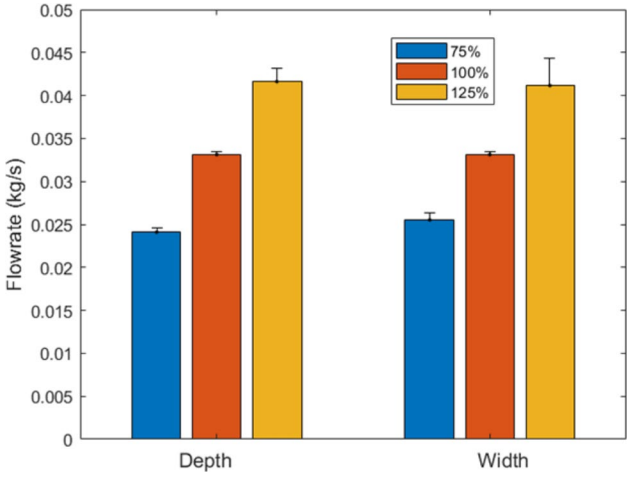

Fig. 8 Flowrate through Channels of Different Depths and Widths. Values averaged across the flexion angles tested (0°- 30°). Percentages are referenced to baseline depth and width values. Error bars represent one standard deviation

in comparison with the smallest depth (75% of baseline). The cross-sectional diameter tended to decrease with increasing flexion. On average, this distance was reduced by 4.4 mm as actuator bending increased from 0° to 30°.

The ANOVA examining the effects of chamber parameters from actuators across the range of simulated bending angles (0–30°) on simulated flowrate through the chamber revealed that depth and width significantly affected flowrate ($p<0.001$, $\eta p^2\geq0.99$). In general, deeper and wider actuators resulted in greater flowrates. The 125% depth actuators had a flowrate 0.018 kg/s greater than the 75% depth actuators, an increase of more than 50% (Fig. 8). The 125% width actuators had a flowrate 0.008 kg/s greater than that of the 75% depth actuators. In contrast, shape and wall thickness did not have a significant effect on flowrate ($p>0.05$).

Hand Exoskeleton bandwidth

The baseline rectangular actuator (1.3-mm wall thickness, width of 9.6 mm, and depth of 9.9 mm) was identified as having the best set of characteristics, with relatively high extension force and low passive bending resistance. Thinner walled actuators could not accommodate the required pressures, while thicker walled actuators had higher passive bending resistance. Wider or deeper actuators, while providing better flowrate, may have difficulty fitting on the hand. Thus, the soft hand exoskeleton was fabricated with these rectangular actuators.

The delay in force generation by the chamber on an external body was examined at a 45° bending angle. The rise time tended to decrease as chamber pressurization increased up to a certain pressure: 1.0, 0.7, 0.4, and 2.1 s for 6.9, 20.7, 34.5, and 48.3 kPa, respectively. At a pressure of 48.3 kPa, the actuator began undergoing expansion of the chamber, which slowed the generation of force such that the fastest force response occurred at 34.5 kPa (0.4 s). We used this pressure to determine that the glove could be used to complete a cycle of grasp and release (voluntary flexion followed by passive extension produced by the glove) in 1.1 s.

Discussion

We designed and fabricated soft actuators which provided substantial finger extension assistance at low inflation pressures. The DS20 actuators created extension forces four times greater than our previous polyurethane actuator [29] and greater joint torque than PVC actuators at half of the input pressure (reported torque of 0.09 Nm at 96 kPa of pressure) [15]. This lower pressure requires less power and space for compressors, valves, and junctures.

Actuator extension force increased with bending angle until 45° of bending and remained relatively constant at greater flexion angles. Channel deformation began forming beyond a bending angle of 30°, but airflow did not appear to be greatly restricted at any tested angle. The increasing extension force with greater finger flexion is a generally desirable trait for assisting finger extension. By design, the actuator produces limited pushing force against the finger when the finger is extended (low flexion angle). The chamber can, however, provide considerable resistance to imposed flexion in that posture, which is beneficial for resisting the involuntary activation of the finger flexor muscles, which is common following stroke. For example, when training individuation in stroke survivors or individuals with CP, it may be desirable to resist flexion of digits that are not instructed to move [29].

Of the parameters tested, actuator shape and wall thickness had the greatest effects on generated finger extension force. A rectangular cross-section led to greater force applied to the artificial finger than the semi-obround profile. Additionally, we saw a trend, albeit marginally insignificant, toward greater extension force creation with greater chamber depth.

To minimize passive resistance to finger flexion, we did not incorporate features such as torque-compensating layers or complex geometries, such as sinusoidal channels [17] or multiple segments [34]. These features could be included in future designs to provide greater extension assistance, although at the cost of resisting desired finger flexion in stroke survivors who may have profound flexor weakness [35].

For our designs, passive bending resistance of the chamber was low on average even at atmospheric pressure (0.15 N). Although passive bending resistance was significantly greater for chambers with rectangular shape than for the semi-obround shape, the absolute increase was small. The largely elastic nature of the resistance suggests that this impedance may help in extending the finger once the user relaxes the flexor muscles. To further decrease passive bending resistance, one could apply vacuum pressure, which reduced passive resistance overall. There was no effect of chamber shape on passive resistance once the vacuum was introduced. Thus, these actuators are sufficiently compliant to accommodate palmar placement so that the chamber can push rather than pull the digit into extension.

The prototype hand exoskeleton we created with these chambers is highly backdrivable (the entire glove can be rolled into a ball) and the components on the hand are very lightweight. They do not impede rotation or translation of the hand in space beyond the limitations imposed by the length of the pneumatic tubes connecting the chambers to external servovalves. While palmar actuator location has been employed for a rigid exoskeleton [27], it is not the norm despite safety and comfort advantages, e.g., the chamber only applies force up to the neutral position for the digit (straight finger), thereby reducing risk of joint hyperextension. This is similar in concept to efforts to assist shoulder abduction and flexion [36] or knee extension [37] through inflation of bladders that push rather than pull the joint. Where rigid components on the palmar side of the hand might interfere with practice of grasp of real objects, the compliant pneumatic chambers allow grasping of objects, as we have demonstrated with our prior pneumatic exoskeleton [38].

A primary concern with the palmar location of pneumatic channels is the restriction of airflow with finger bending. The FEMs revealed that, over the flexion angles simulated, the chamber designs did not experience significant changes in flowrate, despite the apparent chamber deformation due to the bending. This is likely due to the relatively large cross-sectional areas used for these

actuators, especially compared to past PVC actuators [15]. Of course, at greater flexion angles, flow restrictions may become apparent. As the finite element simulations became unstable at these larger flexion angles, airflow could not be quantified.

Overall, we observed the best response for a pneumatic chamber with a rectangular shape and our baseline parameter values. We subsequently constructed a hand exoskeleton using a separate actuator for each digit. With this prototype hand exoskeleton, the user was able to complete a flexion/extension finger movement cycle in 1.1 s, an improvement of more than 50% relative to the time needed to complete this cycle with the custom polyurethane actuator we have been using [39]. This rapid motion cycling permits efficient practice of independent finger movements, enabling potentially thousands of movements within a single therapy session.

This study does have several limitations that temper generalizability of the results. The parameter space for actuator characteristics was not fully explored, with some combinations of characteristics omitted, which may have limited understanding of interactions between multiple actuator characteristics such as width and depth. Only two chamber shapes were examined, although these do represent popular options that are easy to fabricate. We modeled DS20 as an elastic material in SolidWorks, but it can exhibit hyper-elasticity. For the strains we observed, the elastic model seemed sufficient, but hyper-elastic models may be needed in future simulations with greater strains.

The pneumatic actuators presented here hold promise for use in hand exoskeletons to assist desired digit extension and resist unwanted digit flexion. We were able to find an optimal configuration within the explored design parameter space, although other shapes and parameters may further improve performance. Designs typically represented a trade-off between the amount of extension assistance that could be provided and the level of passive resistance to imposed flexion. Different applications may weight these outcomes differently.

Conclusions

We examined the use of easily fabricated pneumatic chambers for assisting joint extension. After exploring the chamber parameter space through both simulation and experimentation, we selected an actuator design that was successfully incorporated into a prototype hand exoskeleton that enabled rapid finger movement for repetitive practice. The chambers are designed for location on the palmar surface of the digit to provide digit extension force in a safe and comfortable manner. For use of the hand exoskeleton with real objects, vacuum pressure could be employed to further flatten the actuators in order to decrease their profile and improve object interaction during grasp. In the future, cyclic loading should be performed to examine the impact of repetitive use on actuator properties, including material fatigue. With their extremely low passive bending resistance, relatively high extension force, and excellent ability to conform to body shape, these actuators hold promise for assisting rotation of the finger joints and potentially other joints as well.

Abbreviations

CP	Cerebral Palsy
DS20	Dragon Skin 20
FEM	Finite Element Model

Acknowledgements

Not applicable.

Author contributions

JM collected and analyzed data and GB assisted with data collection. JM, GB, and DK contributed to the design of the experiments. JM and DK created an original manuscript draft and all three authors edited and revised the manuscript.

Funding

This work was supported in part by grant 5R21HD105874-02 from the NIH (NICHD).

Data availability

Individual data points are displayed in the figures and summary values are provided in the text. The datasets used and/or analyzed during the current study are available from the corresponding author on request.

Declarations

Ethics approval and consent to participate

Not applicable.

Consent for publication

Not applicable.

Competing interests

The authors declare no competing interests.

Received: 5 October 2023 / Accepted: 13 August 2024
Published online: 30 August 2024

References

1. Trombly CA. Stroke, in Occupational therapy for physical dysfunction, C.A. Trombly, Editor. 1989, Williams & Wilkins: Baltimore. p. 454–71.
2. Collaborators GBDS. Global, regional, and national burden of stroke, 1990–2016: a systematic analysis for the global burden of Disease Study 2016. Lancet Neurol. 2019;18(5):439–58.
3. Boehme AK, Esenwa C, Elkind MS. Stroke risk factors, Genetics, and Prevention. Circ Res. 2017;120(3):472–95.
4. Uvebrant P. Hemiplegic cerebral palsy. Aetiology and outcome. Acta Paediatr Scand Suppl. 1988;345:1–100.
5. Fedrizzi E, et al. Hand function in children with hemiplegic cerebral palsy: prospective follow-up and functional outcome in adolescence. Dev Med Child Neurol. 2003;45(2):85–91.
6. Hurley DS, et al. The cerebral palsy research registry: development and progress toward national collaboration in the United States. J Child Neurol. 2011;26(12):1534–41.
7. Kirby RS, et al. Prevalence and functioning of children with cerebral palsy in four areas of the United States in 2006: a report from the Autism and Developmental Disabilities Monitoring Network. Res Dev Disabil. 2011;32(2):462–9.

8. Chiang H, Slobounov SM, Ray W. Practice-related modulations of force enslaving and cortical activity as revealed by EEG. Clin Neurophysiol. 2004;115(5):1033–43.
9. Slobounov S, et al. Modulation of cortical activity as a result of task-specific practice. Neurosci Lett. 2007;421(2):126–31.
10. Wallen M, et al. Modified constraint-induced therapy for children with hemiplegic cerebral palsy: a feasibility study. Dev Neurorehabil. 2008;11(2):124–33.
11. DeLuca SC, et al. Constraint-induced movement therapy (CIMT) for young children with cerebral palsy: effects of therapeutic dosage. J Pediatr Rehabil Med. 2012;5(2):133–42.
12. Stearns GE, et al. Effects of constraint-induced movement therapy on hand skills and muscle recruitment of children with spastic hemiplegic cerebral palsy. NeuroRehabilitation. 2009;24(2):95–108.
13. Gordon AM, et al. Efficacy of a hand-arm bimanual intensive therapy (HABIT) in children with hemiplegic cerebral palsy: a randomized control trial. Dev Med Child Neurol. 2007;49(11):830–8.
14. Charles J, Gordon AM. Development of hand-arm bimanual intensive training (HABIT) for improving bimanual coordination in children with hemiplegic cerebral palsy. Dev Med Child Neurol. 2006;48(11):931–6.
15. Nam C, et al. An Exoneuromusculoskeleton for Self-Help Upper Limb Rehabilitation after Stroke. Soft Robot. 2022;9(1):14–35.
16. Taheri H, et al. Design and preliminary evaluation of the FINGER rehabilitation robot: controlling challenge and quantifying finger individuation during musical computer game play. J Neuroeng Rehabil. 2014;11:10.
17. Yap HK, et al. Characterisation and evaluation of soft elastomeric actuators for hand assistive and rehabilitation applications. J Med Eng Technol. 2016;40(4):199–209.
18. Yap HK, Ng HY, Yeow CH. High-force soft printable pneumatics for soft robotic applications. Soft Rob. 2016;3:144–58.
19. Sun Y, et al. Stiffness customization and patterning for property modulation of silicone-based Soft Pneumatic Actuators. Soft Robot. 2017;4(3):251–60.
20. O'Neill CT, et al. A soft wearable robot for the shoulder: design, characterization, and preliminary testing. IEEE Int Conf Rehabil Robot. 2017;2017:1672–8.
21. Tang ZQ, et al. A probabilistic model-based online learning optimal control algorithm for soft pneumatic actuators. IEEE Rob Autom Lett. 2020;5:1437–44.
22. Polygerinos P, et al. Soft robotic glove for combined assistance and at-home rehabilitation. Rob Autom Syst. 2015;73:135–43.
23. Shapiro Y, Wolf A, Gabor K. Bi-bellows: pneumatic bending actuator. Sens Actuators A: Phys. 2011;167:484–94.
24. Conrad MO, Kamper DG. Isokinetic strength and power deficits in the hand following stroke. Clin Neurophysiol. 2012;123(6):1200–6.
25. McCall JV, Hu X, Kamper DG. Exploring kinetic and kinematic finger individuation capability in children with hemiplegic cerebral palsy. Percept Mot Skills. 2023;130(2):732–49.
26. Koizumi S, et al. Recurrent braiding of Thin McKibben Muscles to overcome their limitation of Contraction. Soft Robot. 2020;7(2):251–8.
27. Bouzit M, et al. The Rutgers Master II-new design force feedback glove. IEEE/ASME Trans Mechatron. 2002;7:256–63.
28. Rad C, Hancu O, Lapusan C. Data-driven kinematic model of PneuNets bending actuators for soft grasping tasks. Actuators. 2022;11.
29. Thielbar KO, et al. Training finger individuation with a mechatronic-virtual reality system leads to improved fine motor control post-stroke. J Neuroeng Rehabil. 2014;11:171.
30. Connelly L, et al. A pneumatic glove and immersive virtual reality environment for hand rehabilitative training after stroke. IEEE Trans Neural Syst Rehabil Eng. 2010;18(5):551–9.
31. McCall JV, Kamper DG. High compliance pneumatic actuators to promote Finger Extension in Stroke survivors. Annu Int Conf IEEE Eng Med Biol Soc. 2021;2021:4588–91.
32. Heung HL, et al. Soft Rehabilitation Actuator with Integrated Post-stroke Finger spasticity evaluation. Front Bioeng Biotechnol. 2020;8:111.
33. Zhang J, et al. Geometric confined pneumatic soft-rigid hybrid actuators. Soft Robot. 2020;7(5):574–82.
34. Heung KHL, et al. Robotic Glove with Soft-Elastic Composite Actuators for assisting activities of Daily Living. Soft Robot. 2019;6(2):289–304.
35. Barry AJ, et al. Characteristics of the severely impaired hand in survivors of stroke with chronic impairments. Top Stroke Rehabil. 2022;29(3):181–91.
36. Proietti T, et al. Restoring arm function with a soft robotic wearable for individuals with amyotrophic lateral sclerosis. Sci Transl Med. 2023;15(681):eadd1504.
37. Sridar S, et al. A soft-inflatable exosuit for knee Rehabilitation: assisting Swing Phase during walking. Front Robot AI. 2018;5:44.
38. Fischer HC, et al. Hand rehabilitation following stroke: a pilot study of assisted finger extension training in a virtual environment. Top Stroke Rehabil. 2007;14(1):1–12.
39. McCall JV, et al. A platform for Rehabilitation of Finger Individuation in children with hemiplegic cerebral palsy. IEEE Int Conf Rehabil Robot. 2019;2019:343–8.

Publisher's Note